T Cell Traction Forces show temporal patterns which Depend on Stimulation and Cell Subtype

Farah Mustapha [1,2,3,4,5], Martine Biarnes-Pelicot [1,2,3,4], Remy Torro [1,2,3,4,5], Jana El Husseiny [1,2,3,4], Kheya Sengupta [4,5,*], Pierre-Henri Puech [1,2,3,4,*]

Affiliations:

Laboratoire Adhésion et Inflammation (LAI)

[1] Aix Marseille University, LAI UM 61, Marseille, F-13288, France.

[2] Inserm, UMR_S 1067, Marseille, F-13288, France.

[3] CNRS, UMR 7333, Marseille, F-13288, France.

CENTURI
[4] Turing Center for Living systems, Marseille, France

Centre Interdisciplinaire de Nanoscience de Marseille (CINAM)
[5] CNRS - AMU UMR 7325, Marseille, F-13288, France

[*] To whom correspondence should be addressed :
kheya.sengupta@cnrs.fr, pierre-henri.puech@inserm.fr

Abstract
T cells use forces to read out and act on the mechanical parameters of their microenvironment, where antigen-presenting cells (APCs) are the most prominent biomechanical partners. Here we explore the early interaction of T cells with an APC-mimicking ultra-soft polymer gel exhibiting physiologically relevant stiffness in the range of 350-450 Pa. We quantify the dependence of cell spreading and stiffness on gel elasticity, and measure early time traction forces. We find that coating the surface with an antibody against the CD3 region of the TCR-complex elicits small but measurable gel deformation in the early recognition phase, which we report as maximal stress and integrated energy. We show that the time evolution of the energy follows one of three distinct patterns: active fluctuations, intermittent, or sigmoidal signals. When using a classical T cell line, we observed that addition of either anti-CD28 or anti-LFA1 has little impact on the total integrated energy or the maximum stress. However, the relative distribution of the energy patterns does depend on the additional ligands. When using primary human T cells, we determined that the subtype and initial state of the cells are strongly affecting the force patterns, in a way that appears coherent with their physiological role.

1 Introduction

T cells are activated when the membrane-bound T cell receptors (TCRs) recognize foreign antigenic peptides presented by the major histocompatibility complexes (pMHCs) of antigen-presenting cells (APCs). This happens within a small cell-cell contact area called the immune synapse (IS) (Grakoui et al., 1999; Monks et al., 1998; Reichardt et al., 2010). This interaction bridges the innate and adaptive immune responses. As the activated T cells multiply, depending on their sub-type, they further differentiate into cytotoxic T cells that directly kill virus-infected and cancer cells, or into helper / regulatory T cells both of which activate and tune the effector functions of other cells in the immune system. There is a growing realization, ever since the pioneering experiments a decade ago (Chen et al., 2014), that functions of T cells are related to their ability to feel, generate, and respond to forces.

Force response is well-studied in other cell types, notably tissue-forming cells such as fibroblasts (Elosegui-Artola et al., 2016; Engler et al., 2006; Geiger & Bershadsky, 2001; Pelham & Wang, 1997; Solon et al., 2007), where it was shown that force is transmitted through well-defined adhesion structures such as focal adhesions, and has an impact on virtually all aspects of cellular physiopathology (Geiger et al., 2009; Janmey et al., 2009; Martino et al., 2018; Schwarz & Safran, 2013; Vogel & Sheetz, 2006).

Immune cells, such as T cells, do not form focal adhesions *per se*, but their ability to generate and respond to forces is at the heart of their function in a variety of situations, ranging from phagocytosis (Herant, 2006; Jaumouillé & Waterman, 2020; Vorselen et al., 2020, 2021) and stop/go signal for migration of leukocytes (Huse, 2017; Jannat et al., 2011; S. H. J. Kim & Hammer, 2021), to antigen extraction and maturation by B cells (A. Kumari et al., 2019; Spillane & Tolar, 2018) and early activation of T cells (Hu & Butte, 2016; Klotzsch & Schütz, 2013; Y. Liu et al., 2016; Thauland et al., 2017). Recent studies show that T cells respond to forces acting at both molecular and cellular scales, and at timescales ranging from seconds to minutes, with outcomes spread over hours, as reviewed in (Basu & Huse, 2017; Huse, 2017; Issler et al., 2023; Limozin & Puech, 2019; Puech & Bongrand, 2021).

At the molecular scale, the modification of the kinetics properties of the pMHC-TCR bond under force is thought to be implicated in its ability to distinguish different peptidic antigens (Y. Chen et al., 2017; Limozin & Puech, 2019). Specifically, bond lifetime, (Ju et al., 2017) rather than the rupture force (Puech et al., 2011), emerges as a potential key parameter, consistent with the TCR/pMHC molecular bond being a slip, rather than a catch bond (Limozin et al., 2019; B. Liu et al., 2021).

The importance of mechanics at the cell scale has also been documented (Hivroz & Saitakis, 2016; Judokusumo et al., 2012; O'Connor et al., 2012; Saitakis et al., 2017; Wahl et al., 2019). Specific mechanical features of immune cells, in particular APCs, can be modulated as a function of the inflammatory conditions (Bufi et al., 2015), and T cells are capable of probing and reacting to this modulation (Judokusumo et al., 2012; O'Connor et al., 2012; Wahl et al., 2019). Interestingly, T cells have also been shown to sense resistance to forces *parallel* to their membrane plane, thus being able to respond to ligand mobility (Comrie et al., 2015; Dillard et al., 2014; Jankowska et al., 2018) as well as readily modulate their global viscoelastic properties in response to local specific signals at very short scales compared to the ones recorded for calcium fluxes, a hallmark of internal signal transduction (Zak et al., 2021).

Traction force microscopy (TFM) has been used to measure cell-scale forces in leukocytes (Henry et al., 2015; Hui et al., 2015; Hui & Upadhyaya, 2017; A. Kumari et al., 2019; Pathni et al., 2022; Ricart et al., 2011), including proof-of-principle measurements on T cells using polylysine nonspecific adhesion in coordination with antibody stimulation to enhance adhesion forces (Hui et al., 2015; Pang et al., 2024). TFM on T cells is particularly challenging when performed in conditions close to physiological ones (Mustapha et al., 2022). First, since they lack specialized adhesion structures such as focal adhesions, and have short contact interaction times with cognate surfaces, the traction force when triggering only specific recognition in early activation steps is

expected to be comparatively low in magnitude and deployed on small, less defined contact zones as compared to that of large fibroblasts or epithelial cells. Second, from a physiological point of view, T cells are very reactive cells and may exist in different initial states, ranging from naive to anergized (i.e. non-reactive state) as a function of their biomechanical history. As a consequence, force amplitude and patterns may differ even within a given cell population. In an effort to meet the challenge, T cell forces have been measured using DNA-force probes (Y. Liu et al., 2016; Ma et al., 2019) and new refined TFM modes are being developed (Lee et al., 2024; Li et al., 2021; Vorselen et al., 2020). Nevertheless, these are yet to be used to their full potential to reveal physiologically relevant time evolution of force application. Moreover, the temporal variations of forces during early T cell contact and activation are rarely dissected in contrast to late time forces, typically after an engagement of circa 30 min (Hui et al., 2015; Pang et al., 2024).

Here we used a classical TFM modality to measure stresses exerted by T cells during the first 15 to 30 minutes of spreading on well-characterized polyacrylamide gels (PAGs) of variable elasticity ranging from ultra-soft (400 Pa) to semi-hard (200 kPa) (Mustapha et al., 2022). We follow, in real-time, the magnitude, and directionality of the stresses generated during the first minutes of T cell engagement with the softest gels whose stiffness is similar to that of non-activated DCs and B cells (Bufi et al., 2015). The cells are specifically engaged *via* the CD3 domain of the TCR complex, in the optional presence of antibodies against the co-receptor CD28, and/or the T cell integrin LFA. Our dynamic force measurements reveal new patterns of force application over time, that are modulated as a function of substrate mechanics, functionalization, and genetic manipulation of cells to introduce fluorescent reporters. Importantly, we show that for primary human T cells from peripheral blood, subtype and initial state impact temporal patterns but not the integrated or maximal force.

2 Results and discussion

Adhesion and spreading depend on gel stiffness, T-cell state and sub-type

Ultra-soft gels with a rigidity comparable to physiological APCs (Bufi et al., 2015) were used as targets. The gels were laterally homogeneous on length scales similar to the T cell size and were doped with fluorescent nanobeads as fiducial markers for following substrate deformations. Previously established protocols (Tse & Engler, 2010) were optimized to obtain films of well-defined and reproducible rigidity, that were thick enough to be both mechanically homogeneous and stable, and thin enough for optical microscopy (Mustapha et al., 2022). The typical thickness of the gels, measured using optical microscopy by focusing on the glass slide and on the upper side of the gel, was ~80µm. The relative intra- and inter-gel variation of elasticity was characterized using AFM microindentation with soft AFM cantilevers decorated with a colloidal-sphere of a radius compatible to typical T cells size **(see SI and SI Fig. S1 and S2 for details)**. The typical thickness of the gels, measured using optical microscopy by focusing on the glass slide and on the upper side of the gel, was ~ 80µm. Using our refined protocol, we are able to produce gels with a very large range of well-defined and reproducible rigidity, quantified as Young modulus (nominal value 400Pa - 200kPa), encompassing the reported range for macrophages and dendritic cells at different moments of the inflammatory process (400Pa-4kPa, (Bufi et al., 2015)).

To quantify the effect of substrate elasticity on cell spreading and mechanics, we seeded Lifeact-GFP transfected Jurkat cells and primary cells on nanobead-free gels of various rigidity, which were surface grafted with aCD3. The apparent spreading area of the cells was quantified, at a given time point, using fluorescence microscopy. Note that though ideally contact area should be measured using a surface technique like reflection interference or total reflection microscopy (Wahl et al., 2019), we observed that our PAA gels are not amenable to either technique due to the image perturbations due to the beads and the index of refraction of the gel. **Fig.1A** shows a sketch of the spreading experiments. The blue band depicts the position at which we set the focus. A typical image of a cell in fluorescence mode is shown, after 20 min of sedimentation and contact and the apparent cell (contact) area was extracted from these images by manual segmentation using Fiji (Schindelin et al., 2012) freehand selection tool **(Fig. 1B)**. The median of the measured area was weakly, but significantly, dependent on substrate elasticity for jurkat cells, the cells having a tendency to spread, on average, more on the softer substrates with rigidity closer to physiological healthy APCs **(Fig. 1 C)**. Interestingly, for Primary T cells on a

given stiffness (chosen to be 20 kPa), the spread area is state and subtype dependent **(Fig. 1 D)**. Collectively, these observations are in good agreement with (Wahl et al., 2019).

Cell stiffness is weakly impacted by gel stiffness, and T-cell state or sub-type

The Young modulus of the cells was measured, after 20 minutes of interacting with the gel surface, by indenting them with a moderate force *via* bead-decorated AFM cantilevers, up to depths of indentation < 1 µm, which represents ~ < 10% of cell diameter **(Fig. 1E,F)**. The measured Young modulus of the order of 100 Pa on gels at physiological range of stiffness was typical for lymphocytes, including Jurkat T cells (Cazaux et al., 2016; Sadoun et al., 2021; Zak et al., 2021) **(Fig. 1G, H)**. Note that it was impossible to reproducibly indent cells on the softest gels due to detachment arising from mechanical perturbations induced by the approach of the AFM cantilever, and those values, when rarely obtained, are therefore not reported. For Jurkat cells, the value of the Young modulus does not show strong variation with substrate elasticity in the gel belonging to the lower elasticity range **(Fig. 1G)**, which could reasonably indicate that the deformation of the gel under the cells can be neglected (Rheinlaender et al., 2020). Pooling data and averaging in this invariant range (namely 2 and 20 kPa), leads to a value of about 100 Pa (see above). On the stiffer gels that do not mimic per se any relevant APC (Bufi et al., 2015), the Young modulus was higher, probably linked to higher spreading, such as what we reported for the effect of relaxing any shape constraint (Sadoun et al., 2021). Nevertheless, the order of magnitude of the Young modulus is still close to the one usually reported values, unlike some very high values reported in recent measurements using dynamic AFM modes (> 10kPa, (Jung et al., 2021)). Interestingly, for Primary T cells on a given stiffness (chosen to be 20 kPa), the naïve, stimulated and memory cells show very different elasticities. Within the category memory however, stimulation has no impact on stiffness **(Fig. 1 H)**.

In the first part of this work, we produced well controlled PAA gels and laterally characterized their mechanical properties using indentation maps in AFM with moderate forces, on scales that are compatible with immune cell dimensions. These properties are homogeneous, tunable over a large range of elasticities, and down to physiological antigen presenting cell ones (Bufi et al., 2015). Such approaches are consistent with the work of others, on B lymphocytes and neutrophils in particular, in terms of gel or substrate elasticity (Henry et al., 2015; A. Kumari et al., 2019, 2020)**.** We used antibody-only substrate decorations, and softer substrates as compared to previous reports on Jurkat cells, where polylysine was used as an underlying layer, which likely increased the spreading of the cells via non-specific, charge-based interactions (Hui et al., 2015). Following our previous work (Dillard et al., 2014; Wahl et al., 2019), here only specific stimuli, in the form of antibodies compatible with primary human cells are used, with nonspecific background interaction being as low and controlled as possible. Note that the PAA gels are intrinsically non-adherent and hence offer low nonspecific interaction (see below for IgG2a coated gels). In absence of any additional nonspecific interaction, spreading is expected to be lower. This should lead to reduced stresses.

T cell forces on ultra-soft gels are elicited only by specific interactions

On **Fig. 2A and SI Fig. S3**, we summarize our strategy for performing traction force microscopy with open-source tools as reported in (Mustapha et al., 2022). To capture the first moments of recognition, image acquisition is started before seeding cells, which allows us to use the first frame of our movies as a reliable reference for the unperturbed state of the nanobeads in the gel. Taking simultaneous images of the cells (fluorescence or transmission) and the nanobeads (fluorescence), we tracked the changes in the position of the nanobeads under a given cell. This was done, after correcting for lateral image drift if any, by calculating the displacement of the beads from the first unperturbed frame at each time point using particle image velocimetry (PIV). By applying Fourier transform traction cytometry (FTTC), we were able to obtain maps of stress vectors, from which we plotted maps of stress-norms for given time points, in order to observe lateral distribution and magnitude of the stress **(See SI and Fig. S3)**. We summarized these series of snap-shots of stress maps into time series of either the sum of the stress-norms over the whole image, ('stress-sum' in Pa), or the scalar product of the displacements and forces at each reconstituted pixel ('Energy' in J). The latter was offset to zero from a

baseline, whose value appeared to be robust between experiments (data not shown), and was defined using the first few time points recorded before the arrival of a cell.

We verified that Jurkat cells generated no significant nanobead motion on IgG2a (as an isotype control) coated gels. In contrast, nearly all cells caused small but visible nanobead displacements when the substrate was coated with the activating antibody aCD3 (Max Stress Sum and Integrated Energy shown in **Fig. 2 B, C**). This demonstrates that the cell-gel interaction is highly specific, and that no non-specific interaction occurs with the PAA, decorated or not with a non-relevant antibody. We shall focus on the time dependent evolution of the Energy (time-energy curves, shaded area on **Fig. 2D**), and the peak value of the stress-sum (Max Stress Sum, dot on **Fig. 2D**). The regularization factor, always required for TFM quantification, was optimized for our experiments **(SI Fig. S4)** and set to the empirically obtained value of $9*10^{-10}$ (Mustapha et al., 2022), which is coherent with previous reports using the same data processing procedure (Tseng et al., 2012). We verified that Jurkat cells generated no significant nanobead motion on IgG2a (isotype control) coated gels. In contrast, nearly all cells cause small but visible nanobead displacements when the substrate was coated with the activating antibody aCD3 (Max Stress Sum and Integrated Energy shown in **Fig. 2 B, C**). This demonstrates that the cell-gel interaction is highly specific, and that no non-specific interaction occurs with the PAA, decorated or not with a non-relevant antibody.

Three distinct temporal patterns of force traction are discernable

Having established the specificity of the force response, we focused on the dynamics of lymphocytes interacting with aCD3 functionalized gels. Interestingly, the time evolution of the energy could be classified into three major, distinct and typical patterns. The first, topmost curve illustrated in **Fig. 2D**, with no cells present or for cells on non-activating surfaces such as IgG2a, low amplitude fluctuations of the order of 10 atto J, are recorded, which was indistinguishable from the noise before seeding of the cells. Next, the first case in presence of cells on activating surface, the signal fluctuates around a relatively low value which is nevertheless higher than the noise detected before arrival of cells, reaching up to about 100 atto J. We call this the active fluctuation case. In the second case, the energy slowly climbs to a high magnitude, of the order of femto J, but then decreases again. We call this an intermittent signal. In the last case, which we call sigmoidal signal, the energy remains low for a while after a cell arrives at the spot and then jumps to a value whose magnitude is large compared to the small fluctuations visible before the arrival of the cell. The energy stays at this high value, of the order of femto J, during the remaining duration of the experiment (15 minutes).

To ascertain that the 'active fluctuation' case was indeed not noise, we analyzed the standard-deviation of the fluctuating energy curves obtained on IgG2a and the aCD3 combinations and compared them to cell-free zones of aCD3 coated gels, since the latter can can be considered to be a robust readout of the noise level of the overall measurements procedure. Interestingly, we observed that in the control case, as for IgG2a, the standard deviation did not vary between before cell seeding or after 20 sec of cell introduction **(Fig. 2E)**. The 20 sec time cut-off corresponds to the typical time needed for the majority of the cells to sediment on the gel in our hands. We can therefore distinguish the signal on IgG2a that we qualify as "passive noise" and the low signal cases on any aCD3 based substrates compositions that we call "active fluctuations", as stated above. Moreover, the observation of only passive, noise-like fluctuations under cells over the duration of the experiment on IgG2a confirms our previous conclusion that, as expected, no interaction occurs between the cell and the surface on the isotype control.

To our knowledge, the time evolution of traction forces was never reported during early spreading events, especially for leukocytes, and such distinct temporal patterns which strongly impact the magnitude of the observables in a given, apparently homogeneous cell population were never analyzed before **(Fig. 2F,G)**.

We note that the fluctuations we observed are reminiscent of the tiptoeing of cells above substrates before the cells make any decision to spread or not (Brodovitch et al., 2013; Pierres et al., 2008). Unfortunately, due to the loss of lateral resolution imposed by the PIV/FTTC methodology, we could not resolve the real lateral size of

the zones where these oscillations were present. Most likely, the active fluctuations could arise due to active dynamics of microvilli, the tip of which is meant to be a mechanosensitive probe of substrates (Brodovitch et al., 2013) which can even penetrate the target cell to probe its mechanics while increasing the effective contact area of the functional structures (H.-R. Kim et al., 2018; Sage et al., 2012). Interestingly, the PIV movies of the 3 behaviors exhibited marked differences in the relative orientation and dynamics of the bead displacements (which will lead to the same behavior of the stress vectors after FTCC calculation). As such, we observed vectors of small norms which orientation was randomly changing between frames for the fluctuating cases, outward vectors at the beginning of the intermittent cases that eventually cancel out after quickly pointing inward for only a few frames, and for sigmoid cases, the vectors were pointing outward and stayed stable for the usual duration of the experiment (15 min).

When extending the observation duration from 15 to 30 min, we observed that some of the cells may change their behavior over time. Below 15 min, they mainly spread, and as consequence the beads below them displace outward **(Suppl. Fig. S5A)**, the resulting stresses pointing also outwards **(Suppl. Fig. S5B)**. The number of PIV calculated pixels exhibiting a displacement above the noise level detected outside the zone below the cells increased with the accumulated energy **(Suppl. Fig. S5C,D).** For longer times, cells start to pull, potentially retract, and bead displacements will point inward, with the resulting stress vectors pointing inwards. Eventually, the cell may stop interacting, or at least, to generate detectable beads motions. This is coherent with the observations made with soft micropillar experiments with different cellular systems (Bashour et al., 2014; Henry et al., 2015; Jin et al., 2019) and using micro-mechanical manipulations (Hu & Butte, 2016; Husson et al., 2011; Sawicka et al., 2017; Thauland et al., 2017)**.** Such a contraction at later times during a contact is reminiscent of typical observation for activating T cells: they stop migrating first, and then change shape by rounding while fully activating; when micro-manipulated against an activating bead or an AFM cantilever, they start to push-pull on the object (Zak et al., 2021).

Temporal patterns of force traction depend on substrate elasticity

We next compared the behavior of the Jurkat cells on CD3 coated substrates with a Young modulus of ~ 400Pa vs ~ 2kPa. Interestingly, we observed that the fraction of the population showing intermittent pulling was dominant on the more rigid gel **(Fig. 2G).** Consequently, the pooled maximal stress sum and integrated energy were lower in this later case **(Suppl. Fig. 2H and I).** The separation of the integrated energies per morphology is shown on **Suppl. Fig. 2J.** These observations underline the necessity of using ultra-soft gels for monitoring the early forces generated by immune cells, and show why using typical gels in the range of 2-5kPa as for adherent cells is surely not optimal: the population pulling intermittently may be missed depending on the moment where the exploration of the samples are performed, leading to the false impression that very little cells are indeed pulling / pushing on the gels, if any.

Temporal patterns of force traction are co-receptor dependent

We next observe and compare the existence of the different regimes in the presence of antibodies against co-receptors such as CD28 and CD11a, in addition to aCD3, using Jurkat cells. In each case, an increase in integrated energy is observed after 20 minutes of interaction **(Suppl. Fig. S6A)**. The median value of the integrated energy is not affected by the presence of CD28, whereas it is lowered in the presence of CD11a. Next, focusing on the distribution of the regime-types **(Suppl. Fig. S6B)**, we see that the distribution of the temporal patterns are, however, co-receptor dependent. Noting that as expected, the integrated energy is lowest for intermittent signals, the lowering of integrated energy in case of aCD3/aCD11a can be understood in terms of increase in occurrence of active fluctuation regime. The limited impact in presence of aCD28 is reminiscent of our recent observation that aCD28 did not strongly influence the spreading area of the same T cell line on soft substrates (Wahl et al., 2019), while it could be different for primary cells (Judokusumo et al., 2012).

Overall, the differences discernable in the occurrence of the different temporal pattern regimes (**Suppl. Fig. S6B**), are hidden when looking at Max Stress Sum averaged over the entire population (**Suppl. Fig. S6C**), and is

similarly minimized when integrated energy is similarly averaged (**Suppl. Fig. S6D**). When the integrated energy for each regime is plotted, the influence of co-receptors is again evident (**Suppl. Fig. S6E**).

Temporal patterns of force traction are impacted by even minor cytoskeletal perturbations

In the experiments reported here so far, Jurkat cells transfected with a cytoskeletal fluorescent reporter (Lifeact-GFP) were used. The use of fluorescent cells for quantification of spreading and the subsequent TFM eases their detection and allows the use of multiband filter sets and diodes for changing the illumination without introducing any mechanical action on the microscope which may perturb the lateral/vertical position of the sample compared to the control image.

However, though often such labeling is used as a simple reporter, without verifying its impact on the biophysical or even biochemical properties of interest, we recognize that they may in fact impact the final readout. We therefore compared LifeAct and WildType cells (**Suppl. Fig. S7**), noting that it is difficult to measure the cell contact area for the latter.

Interestingly, the Lck-GFP variant, which is often used as a simple membrane reporter, appears to behave more like the WT case for the max stress sum, since its cytoskeleton is not affected by the labeling, but shows strong modulations of the energy signal morphologies, towards short lived or only fluctuating ones, and very few sustained, sigmoid signals : this results in a large dispersion of the energies, with very low values and very high ones. (**Suppl. Fig. S8A**). We found that no significant difference is detected in either the pooled maximum stress (**Suppl. Fig. S8B**) or integrated energy (**Suppl. Fig. S8C**). The Lifeact-GFP variant however does have a slightly lower median value of maximal stress than that of the WT, coherent with the impact of intercalating a dye in the actin cytoskeleton, which may impair its capacity to exert local forces.

The distribution of population showing the different temporal pattern types are however impacted by LifeAct-GFP. The fact that stresses and energies morphologies were modified for Lifeact-GFP cells as a comparison to WT cells, in our experiments, is well in line with the observations that Lifeact is not a simple reporter and that its expression can subtly affect the biophysical responses as reported recently (Flores et al., 2019; Sliogeryte et al., 2016). This reveals that the temporal patterns relative frequency is a sensitive observable to detect modulations in force application and sensation by lymphocytes (**Suppl. Fig. S8C,D**).

Temporal patterns of force traction depend on Primary cells subtype

Next we switch to primary human cells which are free of possible artifacts discussed above and in addition offer the possibility of exploring differences between T cell subtypes. Using classical commercial kits, we obtained naive, effector and memory (activated or not) subpopulations of T cells. We also used mixed populations (called pan T cells here). Each subtype was characterized using flow cytometry **(Fig. Supp. S9**). As in our previous TFM experiments, we captured the first moments of the T cells landing and interacting with the aCD3-functionalized 400 Pa PAGs.

By pooling the integrated energies and max forces for each subtype population, we verified that when seeded on aCD3 substrates, all cell subtypes exhibit higher signal than the control case on the control isotype IgG2a **(Fig. 3A, B)**. This indicated that the observed signatures were indeed specific to these very substrates. We observe that both the Max Stress Sum and the Integrated Energy are modulated by the cell subtype (the Integrated Energy varying from atto J to femto J) and are the highest for non-activated memory T cells. Upon activation, both these values decrease for each given subtype. Naive T cells seem to exert negligible force, whereas effector cells exert larger forces which are still a fraction of the values seen for memory cells.

Next, by looking at the morphology of the entire temporal pattern of Integrated Energy, we observed that for each of the different primary T cell populations, the same three regimes described above for Jurkat T cells, namely sigmoidal, intermittent and active fluctuations, were observed **(Fig. 3C)**. In addition, a new identifiable

morphology subtype, similar to a multi-step sigmoidal, was found specifically for the memory T cell subpopulation (not shown here); these cases were henceforth counted under sigmoid regime, since their overall morphology was, on a global scale, close to this main class.

Comparing the distribution of temporal pattern regimes **(Fig. 3 C)**, it is seen that memory T cells exhibited both sigmoidal and intermittent morphologies, while effector T cells exhibit exclusively intermittent morphology, and naive T cells exhibit both intermittent and active fluctuation morphologies. Surprisingly, similar to what we see with the memory T cells, the Pan T cell population, which represents the whole T cell population, combining the naive, effector and memory T cells, exhibits only sigmoidal and intermittent morphologies. As these cells are isolated from donor blood bags, the lack of the active fluctuation morphology, which we only observe in a small percentage (25%) of the naive subset, could be simply attributed to the fact that naive T cells constitute at best 10% of all peripheral blood T cells, which is instead dominated by memory T cells (around >50% ; (Xia et al., 2021)).

Above, we established, using Jurkat cells, that the sigmoidal and intermittent energy curves are correlated with higher levels of integrated energy, opposite to the active fluctuations which reflect the lowest levels of integrated energy. This applies here as well **(Fig. 3C,D)** as the unactivated memory T cells, exhibiting the highest percentage (circa 86%) of sigmoidal curves between the different subtypes, which in turn display significantly higher levels of integrated energy than the remaining subtypes, conversely to the naive T cells - the only subtype comprising active fluctuation energy curves (25 %) - display the lowest (**Fig. 3B**).

The differences in the maximum stresses and integrated energy levels recorded between the memory, effector, and naive T cells, which is indeed reflected in the dispersion of the data points in the Pan T cell population, hint towards the very exciting possibility that force exertion differs based on the action carried out by a specific T cell subtype as a function of time.

In the physiological context, memory T cells have been shown to exert a cytokine (CD4+)/cytotoxic (CD8+) response to re-stimulation by their cognate pMHCs irrespective of the presence of a costimulatory signal (Signal 2). Conversely, a naive T cell will never undergo stimulation and clonal proliferation outside of the lymphoid structures since it requires Signal 1 and Signal 2 from a dedicated APC (Murphy et al., 2008). An attractive hypothesis is that the increased force exertion exhibited by memory T cells upon restimulation,) in comparison to naive T cells, as seen here for aCD3 on soft-as-APC gels, might contribute to their ability to undergo activation much more easily.

3 Conclusions

We presented traction force microscopy experiments with well-characterized ultra-soft poly-acrylamide gels. Using open source software solutions, we quantified the early stresses exerted by model T lymphocytes of the Jurkat cell line and primary human T cells. We quantified the spatio-temporal patterns of these forces. We observed that at early times, while the cell spread, the spatial pattern is described by arrows that point roughly outwards. However, they often reverse direction at later times, with the cells starting to pull on the substrate after about 15 minutes of spreading. This was coherent with reports on neutrophils on a bed of deformable nano-pillars (Henry et al., 2015).

We focused on the early time behavior and followed a temporal pattern of stress and energy. We showed that they can be classified into three distinct regimes, the frequency of each depends on the specific antibody used to coat the gel. One of these regimes consists of enhanced fluctuations as compared to controls, reminiscent of cells tiptoeing on substrates before taking a decision to spread or not (Brodovitch et al., 2013). The two other categories - an intermittent signal, which grows then disappears in the 15 min observation frame, and a sigmoid signal which, once started, lasts until the end of the experiment with the cell reaching a steady state in stress application, were also observed. Such observations of the cell early dynamics stress modulations have not been reported in the literature for T cells or, to our knowledge, any cell type. The distribution of the categories as well as the magnitude of stress or energy are affected by the molecular details of the coating of the gel surface, the stiffness of the gel and even small perturbation of the cytoskeleton.

Interestingly, these different regimes were discernible only when the gel was ultra-soft with stiffness comparable to APCs. On the more common soft gels which are nevertheless stiffer than healthy APCs (Bufi et al., 2015) mainly transient signals were observed. It is worthwhile to note that these regimes were also very sensitive to cytoskeletal modification, including LifeAct transfection. We therefore emphasize that great caution is needed when studying subtle effects in mechanotransduction, especially for sensitive cells such as lymphocytes (Cazaux et al., 2016; Sadoun et al., 2020; Zak et al., 2021).

Using the Jurkat E6.1 cell line allowed us to establish the system but this strategy also has drawbacks. Even though the Jurkat cell line recapitulates some of the hallmark events of T cell activation, there still exists some essential differences between them and primary T cells: E6.1 cells lack the expression of PTEN (phosphatase and tensin homologue) and SHIP (SH2-domain-containing inositol polyphosphate 5' phosphatase), lipid phosphatases that regulate phosphoinositide-3 kinase (PI3K) function (a key molecular regulator of T cell differentiation (Han et al., 2012)). More importantly, from a mechanobiology perspective, E6.1 do not express the force-sensing protein lymphocyte-specific Crk-associated substrate (Cas-L), that has been recently shown to mechanically link TCR MCs to the underlying actin network (Santos et al., 2016). Moreover, the F-actin protrusions that have been readily observed in primary T cells, and which are presumed to play an important role in TCR-pMHC interaction (Cai et al., 2017), have not been documented in Jurkat cells (S. Kumari et al., 2015) These genetic and morphologic distinctions most likely underline the differences found in IS architecture in Jurkat T cells in comparison to primary CD4+ T cells (S. Kumari et al., 2019). In fact, we think that the subtle effects seen above could be more important on primary cells, which may have a different, more subtle, activation history.

Therefore, we also studied human primary T cells subtypes which were activated or not. We observed the Integrated Energy and the Maximum Stress both vary from subset to subset. Additionally, the three temporal regimes identified earlier were present and their distribution was different among the different subsets. Interestingly, it can be hypothesized that the increased force exertion exhibited by memory T cells upon restimulation (in our case by aCD3 on soft-as-APC gels), might contribute to their ability to undergo activation much more easily.

Overall, here we reveal that at early times, and on ultra-soft gels of physiological stiffness, and that the resulting stresses and energies follow three distinct time patterns which are sensitive to subtle biochemical and biophysical factors as well as the initial cell state. Our results provide new insight into early stages of mechanotransduction of lymphocytes.

4 Material and methods

Cells. Human Jurkat T cells (clone E6-1, ATCC TIB-152), as a model for lymphocytes, were obtained from ATCC. Primary cells were purified from blood from healthy volunteers obtained through a formalized agreement with the French Blood Agency (Établissement Français du Sang, agreement 2017-7222), after receiving the informed consent of the donors, in accordance with the Declaration of Helsinki. All experiments were approved by the INSERM Institutional Review Board and the Ethics Committee. For cell culture protocols,purification, sorting transfection details and cytometry experiments, please refer to Supplementary Materials.

Polyacrylamide gels. Fabrication, functionalization and characterization of PAGs (mechanical, by Atomic Force Microscopy indentation, and coating homogeneity by fluorescence microscopy) are summarized in the Supplementary Material and details can be found in (Mustapha et al., 2022).

T cell spreading evaluation. The cells were left to interact with the medium and temperature equilibrated gels for 20 min before image acquisition started. The system was focused just above the gel surface. The obtained images were processed using FijiI/ImageJ (Schindelin et al., 2012) by delineating the contour of the cells to quantify the apparent cell area. All experiments were performed at 37°C.

T cell mechanics using Atomic Force Microscopy. The maximal force to be applied was set at 500 pN for cells, leading to indentation depths of the order of one µm for cells, using a contact duration of 0 sec and the speed of pressing and pulling was $2\mu m.s^{-1}$. Data was typically recorded at 2048 Hz. Up to 5 force curves were recorded for each adhered T cell tested. Data processing using JPK Instrument software is described in the Supplementary Materials. To note, we chose to fit over 0.5 µm of indentation to minimize contributions from the nucleus (Sadoun et al., 2020). All experiments were performed at 37°C.

Traction Force Microscopy (TFM). The optical microscope set-up and the parameters used are summarized in the Supplementary Materials and can be found in (Mustapha et al., 2022). Briefly, to measure the traction forces, movies of live T cells and fluorescent beads were acquired typically every 5 sec for at least 15 min. All experiments were performed at 37°C.

TFM Data processing. TFM movies were processed using a combination of FijiI/ImageJand in-house Python 3.8 functions. Image sequence was performed using an in-house Python code (Mustapha et al., 2022) from nanobeads tracking data generated with Trackmate (Tinevez et al., 2017). The PIV and FTTC calculations were performed using modified versions of Q. Tseng set of functions for FIJI/ImageJ (https://sites.google.com/site/qingzongtseng/), with further plotting and calculations(https://github.com/phpuech/TFM). We used the Anaconda Python distribution (https://www.anaconda.com/). All data analysis was performed on Linux 64 bits machines. The entire procedure is detailed in (Mustapha et al., 2022).

Data visualization and statistics. Data plotting and significance testing were performed on Linux or Windows 64 bits machines using Python, R and/or Graphpad Prism (6 or 7). We used non parametric tests (Kruskal-Wallis / Wilcoxon) by default since our data was observed to be often largely distributed and not gaussian. If not stated otherwise, one data point corresponds to one measurement, that is, either one median value for a gel or a cell (AFM), or the one value calculated for a cell (spreading, TFM). We used ns for $P > 0.05$, * for $P \leq 0.05$, ** for $P \leq 0.01$, *** for $P \leq 0.001$ and **** for $P \leq 0.0001$.

Acknowledgments

Part of this work was supported by institutional grants from INSERM, CNRS and Aix-Marseille University to the LAI and CINAM.

FM was supported by a PhD grant from the European Union's Horizon 2020 research and innovation programme under the Marie Skłodowska-Curie grant agreement 713750, with the financial support of the Regional Council of Provence- Alpes-Côte d'Azur and with of the A*MIDEX (ANR-11-IDEX-0001-02), funded by the Investissements d'Avenir project funded by the French Government, managed by the French National Research Agency (ANR)

RT was supported by a PhD grant from CENTURI (Turing Center for Living systems, Marseille, France), funded from the « Investissements d'Avenir » French Government program managed by the French National Research Agency (ANR-16-CONV-0001) and from Excellence Initiative of Aix-Marseille University - A*MIDEX.

Q. Tseng is aknowledged for his help in using his set of Image J macros, under the form of a shared project in the frame of the CENTURI engineer platform.

We thank L. Limozin and the entire LAI for fruitful discussions and punctual help during this project, P. Pierobon, M. Balland, A. Nicolas and H. Delanoé-Ayari for extremely helpful discussions during the first steps of this work.

The authors thank the INSERM Cell Culture Facility (PCC, Marseille).

Contributions

FM planned and performed the experimental work, analyzed the data and wrote the article, with the help of JEH for primary cell spreading and mechanics. MPB did all cell constructs and helped for cell maintenance and FACS analysis. RT implemented the refined alignment procedure used in the analysis. KS and PHP designed the study, performed some experiments, implemented novel analysis and wrote the article. All co-authors edited the manuscript.

The authors declare no competing interests.

References

Bashour, K. T., Tsai, J., Shen, K., Lee, J.-H., Sun, E., Milone, M. C., Dustin, M. L., & Kam, L. C. (2014). Cross talk between CD3 and CD28 is spatially modulated by protein lateral mobility. *Molecular and cellular biology*, *34*(6), 955–964. https://doi.org/10.1128/MCB.00842-13

Basu, R., & Huse, M. (2017). Mechanical Communication at the Immunological Synapse. *Trends in Cell Biology*, *27*(4), 241–254. https://doi.org/10.1016/j.tcb.2016.10.005

Brodovitch, A., Bongrand, P., & Pierres, A. (2013). T lymphocytes sense antigens within seconds and make a decision within one minute. *Journal of Immunology (Baltimore, Md.: 1950)*, *191*(5), 2064–2071. https://doi.org/10.4049/jimmunol.1300523

Bufi, N., Saitakis, M., Dogniaux, S., Buschinger, O., Bohineust, A., Richert, A., Maurin, M., Hivroz, C., & Asnacios, A. (2015). Human Primary Immune Cells Exhibit Distinct Mechanical Properties that Are Modified by Inflammation. *Biophysical Journal*, *108*(9), 2181–2190. https://doi.org/10.1016/j.bpj.2015.03.047

Cai, E., Marchuk, K., Beemiller, P., Beppler, C., Rubashkin, M. G., Weaver, V. M., Gérard, A., Liu, T.-L., Chen, B.-C., Betzig, E., Bartumeus, F., & Krummel, M. F. (2017). Visualizing dynamic microvillar search and stabilization during ligand detection by T cells. *Science*, *356*(6338), eaal3118–eaal3118. https://doi.org/10.1126/science.aal3118

Cazaux, S., Sadoun, A., Biarnes-Pelicot, M., Martinez, M., Obeid, S., Bongrand, P., Limozin, L., & Puech, P.-H. (2016). Synchronizing atomic force microscopy force mode and fluorescence microscopy in real time for immune cell stimulation and activation studies. *Ultramicroscopy*, *160*, 168–181. https://doi.org/10.1016/j.ultramic.2015.10.014

Chen, B.-C., Legant, W. R., Wang, K., Shao, L., Milkie, D. E., Davidson, M. W., Janetopoulos, C., Wu, X. S., Hammer, J. A., Liu, Z., English, B. P., Mimori-Kiyosue, Y., Romero, D. P., Ritter, A. T., Lippincott-Schwartz, J., Fritz-Laylin, L., Mullins, R. D., Mitchell, D. M., Bembenek, J. N., … Betzig, E. (2014). Lattice light-sheet microscopy : Imaging molecules to embryos at high spatiotemporal resolution. *Science*, *346*(6208), 1257998. https://doi.org/10.1126/science.1257998

Chen, Y., Ju, L., Rushdi, M., Ge, C., & Zhu, C. (2017). Receptor-mediated cell mechanosensing. *Molecular Biology of the Cell*, *28*(23), 3134–3155. https://doi.org/10.1091/mbc.E17-04-0228

Comrie, W. A., Babich, A., & Burkhardt, J. K. (2015). F-actin flow drives affinity maturation and spatial organization of LFA-1 at the immunological synapse. *The Journal of Cell Biology*, *208*(4), 475–491. https://doi.org/10.1083/jcb.201406121

Dillard, P., Varma, R., Sengupta, K., & Limozin, L. (2014). Ligand-Mediated Friction Determines Morphodynamics of Spreading T Cells. *Biophysical Journal*, *107*(11), 2629–2638. https://doi.org/10.1016/j.bpj.2014.10.044

Elosegui-Artola, A., Oria, R., Chen, Y., Kosmalska, A., Pérez-González, C., Castro, N., Zhu, C., Trepat, X., & Roca-Cusachs, P. (2016). Mechanical regulation of a molecular clutch defines force transmission and transduction in response to matrix rigidity. *Nature Cell Biology*, *18*(5), 540–548. https://doi.org/10.1038/ncb3336

Engler, A. J., Sen, S., Sweeney, H. L., & Discher, D. E. (2006). Matrix Elasticity Directs Stem Cell Lineage Specification. *Cell*, *126*(4), 677–689. https://doi.org/10.1016/j.cell.2006.06.044

Flores, L. R., Keeling, M. C., Zhang, X., Sliogeryte, K., & Gavara, N. (2019). Lifeact-TagGFP2 alters F-actin organization, cellular morphology and biophysical behaviour. *Scientific Reports*, *9*(1). https://doi.org/10.1038/s41598-019-40092-w

Geiger, B., & Bershadsky, A. (2001). Assembly and mechanosensory function of focal contacts. *Curr Opin Cell Biol*, *13*(5), 584–592.

Geiger, B., Spatz, J. P., & Bershadsky, A. D. (2009). Environmental sensing through focal adhesions. *Nature Reviews Molecular Cell Biology*, *10*(1), 21–33. https://doi.org/10.1038/nrm2593

Grakoui, A., Bromley, S. K., Sumen, C., Davis, M. M., Shaw, A. S., Allen, P. M., & Dustin, M. L. (1999). The immunological synapse : A molecular machine controlling T cell activation. *Science*, *285*(5425), 221–227.

Han, S. J., Bielawski, K. S., Ting, L. H., Rodriguez, M. L., & Sniadecki, N. J. (2012). Decoupling Substrate Stiffness, Spread Area, and Micropost Density : A Close Spatial Relationship between Traction Forces and Focal Adhesions. *Biophysical Journal*, *103*(4), 640–648. https://doi.org/10.1016/j.bpj.2012.07.023

Henry, S. J., Chen, C. S., Crocker, J. C., & Hammer, D. A. (2015). Protrusive and Contractile Forces of Spreading Human Neutrophils. *Biophysical Journal*, *109*(4), 699–709. https://doi.org/10.1016/j.bpj.2015.05.041

Herant, M. (2006). Mechanics of neutrophil phagocytosis : Experiments and quantitative models. *Journal of Cell Science*, *119*(9), 1903–1913. https://doi.org/10.1242/jcs.02876

Hivroz, C., & Saitakis, M. (2016). Biophysical Aspects of T Lymphocyte Activation at the Immune Synapse.

Frontiers in Immunology, *7*. https://doi.org/10.3389/fimmu.2016.00046
Hu, K. H., & Butte, M. J. (2016). T cell activation requires force generation. *The Journal of Cell Biology*, *213*(5), 535–542. https://doi.org/10.1083/jcb.201511053
Hui, K. L., Balagopalan, L., Samelson, L. E., & Upadhyaya, A. (2015). Cytoskeletal forces during signaling activation in Jurkat T-cells. *Molecular Biology of the Cell*, *26*(4), 685–695. https://doi.org/10.1091/mbc.E14-03-0830
Hui, K. L., & Upadhyaya, A. (2017). Dynamic microtubules regulate cellular contractility during T-cell activation. *Proceedings of the National Academy of Sciences*, *114*(21), E4175–E4183. https://doi.org/10.1073/pnas.1614291114
Huse, M. (2017). Mechanical forces in the immune system. *Nature Reviews Immunology*, *17*(11), 679–690. https://doi.org/10.1038/nri.2017.74
Husson, J., Chemin, K., Bohineust, A., Hivroz, C., & Henry, N. (2011). Force Generation upon T Cell Receptor Engagement. *PLoS ONE*, *6*(5), e19680. https://doi.org/10.1371/journal.pone.0019680
Issler, M., Colin-York, H., & Fritzsche, M. (2023). Quantifying Immune Cell Force Generation Using Traction Force Microscopy. In C. T. Baldari & M. L. Dustin (Éds.), *The Immune Synapse : Methods and Protocols* (p. 363–373). Springer US. https://doi.org/10.1007/978-1-0716-3135-5_23
Jankowska, K. I., Williamson, E. K., Roy, N. H., Blumenthal, D., Chandra, V., Baumgart, T., & Burkhardt, J. K. (2018). Integrins Modulate T Cell Receptor Signaling by Constraining Actin Flow at the Immunological Synapse. *Frontiers in Immunology*, *9*. https://doi.org/10.3389/fimmu.2018.00025
Janmey, P. A., Winer, J. P., Murray, M. E., & Wen, Q. (2009). The hard life of soft cells. *Cell Motility and the Cytoskeleton*, *66*(8), 597–605. https://doi.org/10.1002/cm.20382
Jannat, R. A., Dembo, M., & Hammer, D. A. (2011). Traction Forces of Neutrophils Migrating on Compliant Substrates. *Biophysical Journal*, *101*(3), 575–584. https://doi.org/10.1016/j.bpj.2011.05.040
Jaumouillé, V., & Waterman, C. M. (2020). Physical Constraints and Forces Involved in Phagocytosis. *Frontiers in Immunology*, *11*. https://doi.org/10.3389/fimmu.2020.01097
Jin, W., Tamzalit, F., Chaudhuri, P. K., Black, C. T., Huse, M., & Kam, L. C. (2019). T cell activation and immune synapse organization respond to the microscale mechanics of structured surfaces. *Proceedings of the National Academy of Sciences*, *116*(40), 19835–19840. https://doi.org/10.1073/pnas.1906986116
Ju, L., Chen, Y., Li, K., Yuan, Z., Liu, B., Jackson, S. P., & Zhu, C. (2017). Dual Biomembrane Force Probe enables single-cell mechanical analysis of signal crosstalk between multiple molecular species. *Scientific Reports*, *7*(1). https://doi.org/10.1038/s41598-017-13793-3
Judokusumo, E., Tabdanov, E., Kumari, S., Dustin, M. L., & Kam, L. C. (2012). Mechanosensing in T lymphocyte activation. *Biophysical Journal*, *102*(2), L5-7. https://doi.org/10.1016/j.bpj.2011.12.011
Jung, P., Zhou, X., Iden, S., Bischoff, M., & Qu, B. (2021). T cell stiffness is enhanced upon formation of immunological synapse. *eLife*, *10*, e66643. https://doi.org/10.7554/eLife.66643
Kim, H.-R., Mun, Y., Lee, K.-S., Park, Y.-J., Park, J.-S., Park, J.-H., Jeon, B.-N., Kim, C.-H., Jun, Y., Hyun, Y.-M., Kim, M., Lee, S.-M., Park, C.-S., Im, S.-H., & Jun, C.-D. (2018). T cell microvilli constitute immunological synaptosomes that carry messages to antigen-presenting cells. *Nature Communications*, *9*(1). https://doi.org/10.1038/s41467-018-06090-8
Kim, S. H. J., & Hammer, D. A. (2021). Integrin cross-talk modulates stiffness-independent motility of CD4+ T lymphocytes. *Molecular Biology of the Cell*, *32*(18), 1749–1757. https://doi.org/10.1091/mbc.E21-03-0131
Klotzsch, E., & Schütz, G. J. (2013). Improved Ligand Discrimination by Force-Induced Unbinding of the T Cell Receptor from Peptide-MHC. *Biophysical journal*, *104*(8), 1670–1675. https://doi.org/10.1016/j.bpj.2013.03.023
Kumari, A., Pineau, J., Lennon-Duménil, A.-M., Balland, M., & Pierobon, P. (2020). Traction Force Microscopy to Study B Lymphocyte Activation. *JoVE (Journal of Visualized Experiments)*, *161*, e60947. https://doi.org/10.3791/60947
Kumari, A., Pineau, J., Sáez, P. J., Maurin, M., Lankar, D., San Roman, M., Hennig, K., Boura, V. F., Voituriez, R., Karlsson, M. C. I., Balland, M., Lennon Dumenil, A.-M., & Pierobon, P. (2019). Actomyosin-driven force patterning controls endocytosis at the immune synapse. *Nature Communications*, *10*(1), 2870. https://doi.org/10.1038/s41467-019-10751-7
Kumari, S., Colin-York, H., Irvine, D. J., & Fritzsche, M. (2019). Not All T Cell Synapses Are Built the Same Way. *Trends in Immunology*. https://doi.org/10.1016/j.it.2019.09.009
Kumari, S., Depoil, D., Martinelli, R., Judokusumo, E., Carmona, G., Gertler, F. B., Kam, L. C., Carman, C. V., Burkhardt, J. K., Irvine, D. J., Dustin, M. L., States, U., States, U., De-, N., Sciences, M., Kingdom, U., Israel, B., Medical, D., States, U., … States, U. (2015). *Actin foci facilitate activation of the phospholipase C- γ in primary T lymphocytes via the WASP pathway*. 1–31. https://doi.org/10.7554/eLife.04953
Lee, M., Jeong, H., Lee, C., Lee, M. J., Delmo, B. R., Heo, W. D., Shin, J. H., & Park, Y. (2024).

High-resolution assessment of multidimensional cellular mechanics using label-free refractive-index traction force microscopy. *Communications Biology*, *7*(1), Article 1. https://doi.org/10.1038/s42003-024-05788-4

Li, D., Colin-York, H., Barbieri, L., Javanmardi, Y., Guo, Y., Korobchevskaya, K., Moeendarbary, E., Li, D., & Fritzsche, M. (2021). Astigmatic traction force microscopy (aTFM). *Nature Communications*, *12*(1), Article 1. https://doi.org/10.1038/s41467-021-22376-w

Limozin, L., Bridge, M., Bongrand, P., Dushek, O., van der Merwe, P. A., & Robert, P. (2019). TCR-pMHC kinetics under force in a cell-free system show no intrinsic catch bond, but a minimal encounter duration before binding. *Proceedings of the National Academy of Sciences of the United States of America*, *116*(34), 16943‑16948. https://doi.org/10.1073/pnas.1902141116

Limozin, L., & Puech, P.-H. (2019). Membrane Organization and Physical Regulation of Lymphocyte Antigen Receptors : A Biophysicist's Perspective. *The Journal of Membrane Biology*, *252*(4‑5), 397‑412. https://doi.org/10.1007/s00232-019-00085-2

Liu, B., Kolawole, E. M., & Evavold, B. D. (2021). Mechanobiology of T Cell Activation : To Catch a Bond. *Annual Review of Cell and Developmental Biology*, *37*(1), 65‑87. https://doi.org/10.1146/annurev-cellbio-120219-055100

Liu, Y., Blanchfield, L., Ma, V. P.-Y., Andargachew, R., Galior, K., Liu, Z., Evavold, B., & Salaita, K. (2016). DNA-based nanoparticle tension sensors reveal that T-cell receptors transmit defined pN forces to their antigens for enhanced fidelity. *Proceedings of the National Academy of Sciences*, *113*(20), 5610‑5615. https://doi.org/10.1073/pnas.1600163113

Ma, R., Kellner, A. V., Ma, V. P.-Y., Su, H., Deal, B. R., Brockman, J. M., & Salaita, K. (2019). DNA probes that store mechanical information reveal transient piconewton forces applied by T cells. *Proceedings of the National Academy of Sciences*, *116*(34), 16949‑16954. https://doi.org/10.1073/pnas.1904034116

Martino, F., Perestrelo, A. R., Vinarský, V., Pagliari, S., & Forte, G. (2018). Cellular Mechanotransduction : From Tension to Function. *Frontiers in Physiology*, *9*. https://www.frontiersin.org/article/10.3389/fphys.2018.00824

Monks, C. R. F., Freiberg, B. A., Kupfer, H., Sciaky, N., & Kupfer, A. (1998). Three-dimensional segregation of supramolecular activation clusters in T cells. *Nature*, *395*(6697), 82‑86. https://doi.org/10.1038/25764

Murphy, K., Travers, P., & Walport, M. (2008). *Janeway's Immunobiology 7th Edition* (G. Science, Éd.).

Mustapha, F., Sengupta, K., & Puech, P.-H. (2022). Protocol for measuring weak cellular traction forces using well-controlled ultra-soft polyacrylamide gels. *STAR Protocols*, *3*(1), 101133. https://doi.org/10.1016/j.xpro.2022.101133

O'Connor, R. S., Hao, X., Shen, K., Bashour, K., Akimova, T., Hancock, W. W., Kam, L. C., & Milone, M. C. (2012). Substrate rigidity regulates human T cell activation and proliferation. *Journal of immunology (Baltimore, Md. : 1950)*, *189*(3), 1330‑1339. https://doi.org/10.4049/jimmunol.1102757

Pang, R., Sun, W., Yang, Y., Wen, D., Lin, F., Wang, D., Li, K., Zhang, N., Liang, J., Xiong, C., & Liu, Y. (2024). PIEZO1 mechanically regulates the antitumour cytotoxicity of T lymphocytes. *Nature Biomedical Engineering*, 1‑15. https://doi.org/10.1038/s41551-024-01188-5

Pathni, A., Özçelikkale, A., Rey-Suarez, I., Li, L., Davis, S., Rogers, N., Xiao, Z., & Upadhyaya, A. (2022). Cytotoxic T Lymphocyte Activation Signals Modulate Cytoskeletal Dynamics and Mechanical Force Generation. *Frontiers in Immunology*, *13*, 779888. https://doi.org/10.3389/fimmu.2022.779888

Pelham, R. J., & Wang, Y. (1997). Cell locomotion and focal adhesions are regulated by substrate flexibility. *Proceedings of the National Academy of Sciences*, *94*(25), 13661‑13665. https://doi.org/10.1073/pnas.94.25.13661

Pierres, A., Benoliel, A.-M., Touchard, D., & Bongrand, P. (2008). How cells tiptoe on adhesive surfaces before sticking. *Biophysical journal*, *94*(10), 4114‑4122. https://doi.org/10.1529/biophysj.107.125278

Puech, P.-H., & Bongrand, P. (2021). Mechanotransduction as a major driver of cell behaviour : Mechanisms, and relevance to cell organization and future research. *Open Biology*, *11*(11), 210256. https://doi.org/10.1098/rsob.210256

Puech, P.-H., Nevoltris, D., Robert, P., Limozin, L., Boyer, C., & Bongrand, P. (2011). Force Measurements of TCR/pMHC Recognition at T Cell Surface. *PLoS ONE*, *6*(7), e22344. https://doi.org/10.1371/journal.pone.0022344

Reichardt, P., Dornbach, B., & Gunzer, M. (2010). APC, T cells, and the immune synapse. *Current Topics in Microbiology and Immunology*, *340*, 229‑249. https://doi.org/10.1007/978-3-642-03858-7_12

Rheinlaender, J., Dimitracopoulos, A., Wallmeyer, B., Kronenberg, N. M., Chalut, K. J., Gather, M. C., Betz, T., Charras, G., & Franze, K. (2020). Cortical cell stiffness is independent of substrate mechanics. *Nature Materials*, *19*(9), 1019‑1025. https://doi.org/10.1038/s41563-020-0684-x

Ricart, B. G., Yang, M. T., Hunter, C. A., Chen, C. S., & Hammer, D. A. (2011). Measuring Traction Forces of Motile Dendritic Cells on Micropost Arrays. *Biophysical Journal*, *101*(11), 2620‑2628. https://doi.org/10.1016/j.bpj.2011.09.022

Sadoun, A., Biarnes-Pelicot, M., Ghesquiere-Dierickx, L., Wu, A., Théodoly, O., Limozin, L., Hamon, Y., & Puech, P.-H. (2020). Controlling T cells shape, mechanics and activation by micropatterning. *bioRxiv*, 2020.09.15.295964. https://doi.org/10.1101/2020.09.15.295964

Sadoun, A., Biarnes-Pelicot, M., Ghesquiere-Dierickx, L., Wu, A., Théodoly, O., Limozin, L., Hamon, Y., & Puech, P.-H. (2021). Controlling T cells spreading, mechanics and activation by micropatterning. *Scientific Reports*, *11*(1), 6783. https://doi.org/10.1038/s41598-021-86133-1

Sage, P. T., Varghese, L. M., Martinelli, R., Sciuto, T. E., Kamei, M., Dvorak, A. M., Springer, T. A., Sharpe, A. H., & Carman, C. V. (2012). Antigen Recognition Is Facilitated by Invadosome-like Protrusions Formed by Memory/Effector T Cells. *The Journal of Immunology*, *188*(8), 3686–3699. https://doi.org/10.4049/jimmunol.1102594

Saitakis, M., Dogniaux, S., Goudot, C., Bufi, N., Asnacios, S., Maurin, M., Randriamampita, C., Asnacios, A., & Hivroz, C. (2017). Different TCR-induced T lymphocyte responses are potentiated by stiffness with variable sensitivity. *eLife*, *6*. https://doi.org/10.7554/eLife.23190

Santos, L. C., Blair, D. A., Kumari, S., Cammer, M., Iskratsch, T., Herbin, O., Alexandropoulos, K., Dustin, M. L., & Sheetz, M. P. (2016). Actin polymerization-dependent activation of Cas-L promotes immunological synapse stability. *Immunology and Cell Biology*, *94*(10), 981–993. https://doi.org/10.1038/icb.2016.61

Sawicka, A., Babataheri, A., Dogniaux, S., Barakat, A. I., Gonzalez-Rodriguez, D., Hivroz, C., & Husson, J. (2017). Micropipette force probe to quantify single-cell force generation : Application to T-cell activation. *Molecular Biology of the Cell*, *28*(23), 3229–3239. https://doi.org/10.1091/mbc.E17-06-0385

Schindelin, J., Arganda-Carreras, I., Frise, E., Kaynig, V., Longair, M., Pietzsch, T., Preibisch, S., Rueden, C., Saalfeld, S., Schmid, B., Tinevez, J.-Y., White, D. J., Hartenstein, V., Eliceiri, K., Tomancak, P., & Cardona, A. (2012). Fiji : An open-source platform for biological-image analysis. *Nature Methods*, *9*(7), 676–682. https://doi.org/10.1038/nmeth.2019

Schwarz, U. S., & Safran, S. A. (2013). Physics of adherent cells. *Reviews of Modern Physics*, *85*(3), 1327–1381. https://doi.org/10.1103/RevModPhys.85.1327

Sliogeryte, K., Thorpe, S. D., Wang, Z., Thompson, C. L., Gavara, N., & Knight, M. M. (2016). Differential effects of LifeAct-GFP and actin-GFP on cell mechanics assessed using micropipette aspiration. *Journal of Biomechanics*, *49*(2), 310–317. https://doi.org/10.1016/j.jbiomech.2015.12.034

Solon, J., Levental, I., Sengupta, K., Georges, P. C., & Janmey, P. A. (2007). Fibroblast adaptation and stiffness matching to soft elastic substrates. *Biophysical Journal*, *93*(12), 4453–4461. https://doi.org/10.1529/biophysj.106.101386

Spillane, K. M., & Tolar, P. (2018). Mechanics of antigen extraction in the B cell synapse. *Molecular Immunology*, *101*, 319–328. https://doi.org/10.1016/j.molimm.2018.07.018

Thauland, T. J., Hu, K. H., Bruce, M. A., & Butte, M. J. (2017). Cytoskeletal adaptivity regulates T cell receptor signaling. *Science Signaling*, *10*(469), eaah3737. https://doi.org/10.1126/scisignal.aah3737

Tinevez, J.-Y., Perry, N., Schindelin, J., Hoopes, G. M., Reynolds, G. D., Laplantine, E., Bednarek, S. Y., Shorte, S. L., & Eliceiri, K. W. (2017). TrackMate : An open and extensible platform for single-particle tracking. *Methods (San Diego, Calif.)*, *115*, 80–90. https://doi.org/10.1016/j.ymeth.2016.09.016

Tse, J. R., & Engler, A. J. (2010). Preparation of Hydrogel Substrates with Tunable Mechanical Properties. *Current Protocols in Cell Biology*, *47*(1), 10.16.1-10.16.16. https://doi.org/10.1002/0471143030.cb1016s47

Tseng, Q., Duchemin-Pelletier, E., Deshiere, A., Balland, M., Guillou, H., Filhol, O., & Théry, M. (2012). Spatial organization of the extracellular matrix regulates cell-cell junction positioning. *Proceedings of the National Academy of Sciences of the United States of America*, *109*(5), 1506–1511. https://doi.org/10.1073/pnas.1106377109

Vogel, V., & Sheetz, M. (2006). Local force and geometry sensing regulate cell functions. *Nature Reviews Molecular Cell Biology*, *7*(4), 265–275. https://doi.org/10.1038/nrm1890

Vorselen, D., Barger, S. R., Wang, Y., Cai, W., Theriot, J. A., Gauthier, N. C., & Krendel, M. (2021). Phagocytic 'teeth' and myosin-II 'jaw' power target constriction during phagocytosis. *eLife*, *10*, e68627. https://doi.org/10.7554/eLife.68627

Vorselen, D., Wang, Y., de Jesus, M. M., Shah, P. K., Footer, M. J., Huse, M., Cai, W., & Theriot, J. A. (2020). Microparticle traction force microscopy reveals subcellular force exertion patterns in immune cell–target interactions. *Nature Communications*, *11*(1). https://doi.org/10.1038/s41467-019-13804-z

Wahl, A., Dinet, C., Dillard, P., Nassereddine, A., Puech, P.-H., Limozin, L., & Sengupta, K. (2019). Biphasic mechanosensitivity of T cell receptor-mediated spreading of lymphocytes. *Proceedings of the National Academy of Sciences*, *116*(13), 5908–5913. https://doi.org/10.1073/pnas.1811516116

Xia, Y., Liu, A., Li, W., Liu, Y., Zhang, G., Ye, S., Zhao, Z., Shi, J., Jia, Y., Liu, X., Guo, Y., Chen, H., & Yu, J. (2021). Reference range of naïve T and T memory lymphocyte subsets in peripheral blood of healthy adult. *Clinical and Experimental Immunology*, uxab038. https://doi.org/10.1093/cei/uxab038

Zak, A., Merino-Cortés, S. V., Sadoun, A., Mustapha, F., Babataheri, A., Dogniaux, S., Dupré-Crochet, S., Hudik, E., He, H.-T., Barakat, A. I., Carrasco, Y. R., Hamon, Y., Puech, P.-H., Hivroz, C., Nüsse, O., & Husson, J. (2021). Rapid viscoelastic changes are a hallmark of early leukocyte activation. *Biophysical Journal*, *120*(9), 1692–1704. https://doi.org/10.1016/j.bpj.2021.02.042

Figures captions

Fig. 1: T cell spreading on gels and mechanical properties A: Schematics of the spreading experiments on antiCD3 coated gels of variable rigidity, the colored zone indicates the focal plane position to measure the cell's apparent area. B: Micrograph of a Lifeact-GFP cell showing the presence of cellular extensions. C: Quantification of the apparent area of Jurkat cells on the different substrates. Note that this area is *not* the contact area per se. Typically ~ 200 cells were imaged in total per case. D. Spreading of primary T cells on 20kPa gel as a function of their subtype. E: Schematics of the AFM indentation experiments on cells adhered on similar substrates as for spreading experiments. F: Micrograph showing the bead (white round spot) glued on the cantilever (dark gray triangle) in close proximity to a cell. G: Young modulus measurements of Jurkat cells as a function of substrate rigidity. The Young modulus could not be measured correctly on cells adhered on the softest substrate (see text). H. Young modulus of primary T cells on 20 kPa gel as a function of their subtype. Typically ~20 cells were used per condition. Note that all data presented in Fig. 1G-H was obtained on nanobead-free gels.

Fig. 2 : Traction Force Microscopy, method and application to the biophysics of early Jurkat interactions. A: TFM experiment schematics, with the reference image taken before cell landing. B: Max stress sum of Jurkat cells interacting with aCD3 vs isotype control antibody showing the specificity of the interaction. C. Corresponding Integrated energies. D : Quantification of the SD of the fluctuating curves obtained for different coatings, at the very beginning of the experiments, where the cells are not exerting forces, and later, when they may do. This shows that fluctuating curves observed for bare or IgG2a coated substrates and aCD3 based ones are different, the latter exhibiting larger fluctuations of energy more likely due to cell interactions. E. Time traces of the energy showing the typical temporal patterns observed in absence [top panel] or presence [bottom 3 panels] of specific cellular interaction. F: Relative occurrence of the types of curves obtained in the different situations with antibody decorated substrates. G: Integrated energy over the time of the experiment (15 min) of curve type for aCD3 substrates. H: Relative occurrence of energy curve morphology for the same cell preparations seeded on gels of two gels of different rigidities, coated with aCD3. Color code is the same as in Fig. 2F. I: Pooled max stress sum and J: Pooled integrated energy for cells sitting on these gels. K: Same data separated by curve morphology and gel elasticity.

Fig. 3 : Traction Force Microscopy of primary human cells A. : Pooled maximum of the sum of stresses as a function of substrate coating. B: Pooled integrated energy over the time of the experiment (15 min). Each point corresponds to a cell, the bar presents the median of the data. C: The relative occurrence of the different energy curve morphologies obtained for the displayed T cell subsets. Color code is the same as in Fig. 2F. D : Separation of the different morphologies for the cell subsets.

Graphical abstract

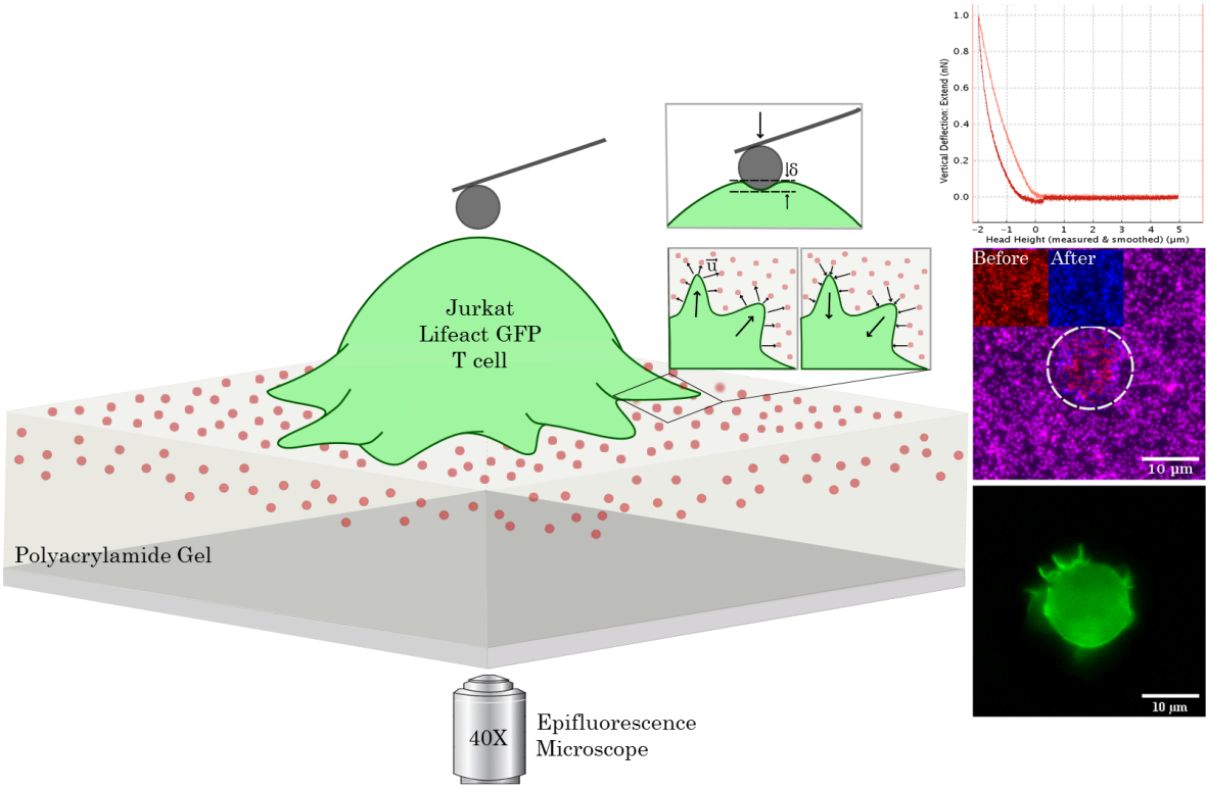

Figure 1

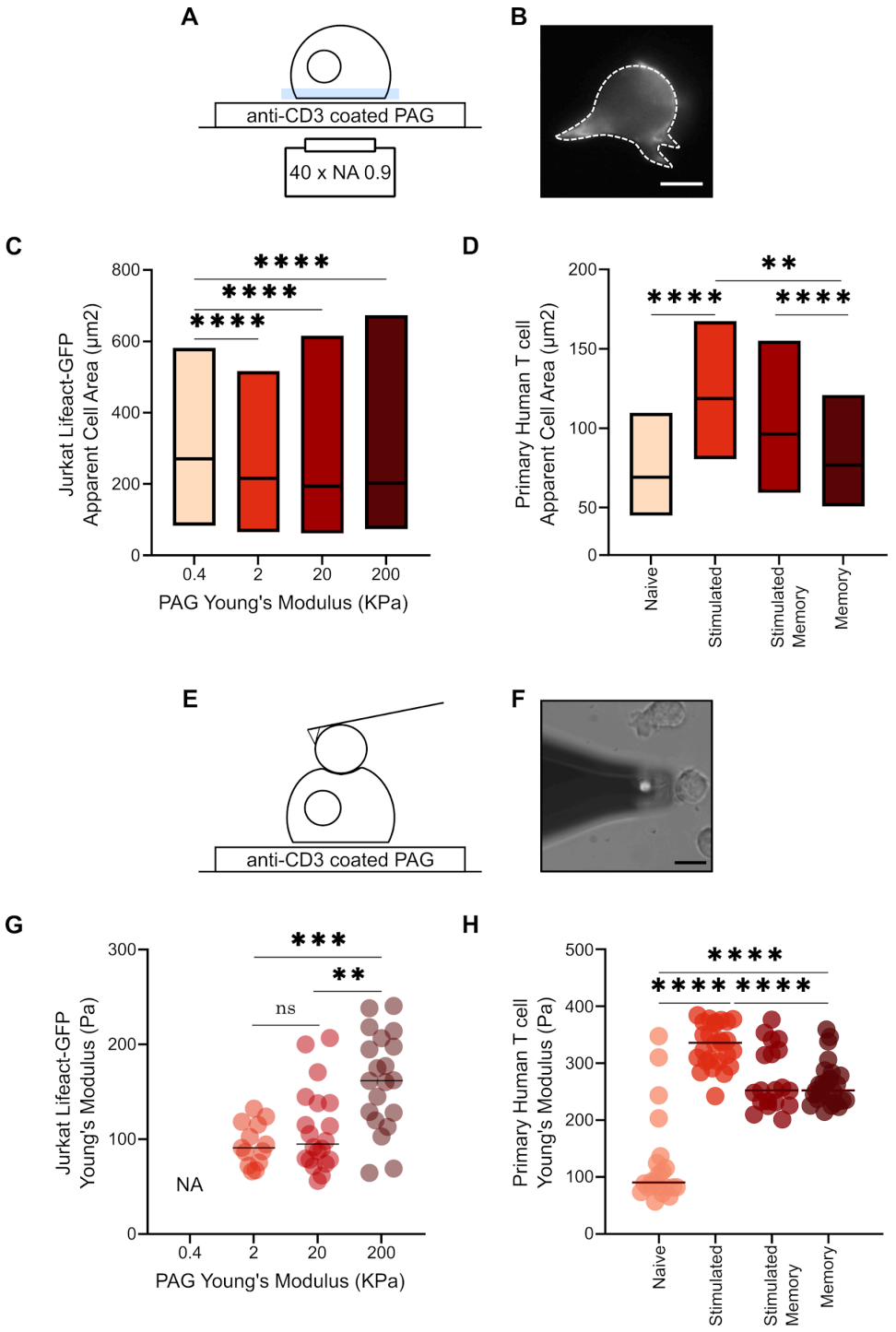
A
anti-CD3 coated PAG
40 x NA 0.9
B
C
Jurkat Lifeact-GFP
Apparent Cell Area (µm2)
800
600
400
200
0
****
****
****
0.4
2
20
200
PAG Young's Modulus (KPa)
D
Primary Human T cell
Apparent Cell Area (µm2)
200
150
100
50
0
**
****
****
Naive
Stimulated
Stimulated Memory
Memory
E
anti-CD3 coated PAG
F
G
Jurkat Lifeact-GFP
Young's Modulus (Pa)
300
200
100
0
***
**
ns
NA
0.4
2
20
200
PAG Young's Modulus (KPa)
H
Primary Human T cell
Young's Modulus (Pa)
500
400
300
200
100
0
****
**** ****
Naive
Stimulated
Stimulated Memory
Memory

Figure 2

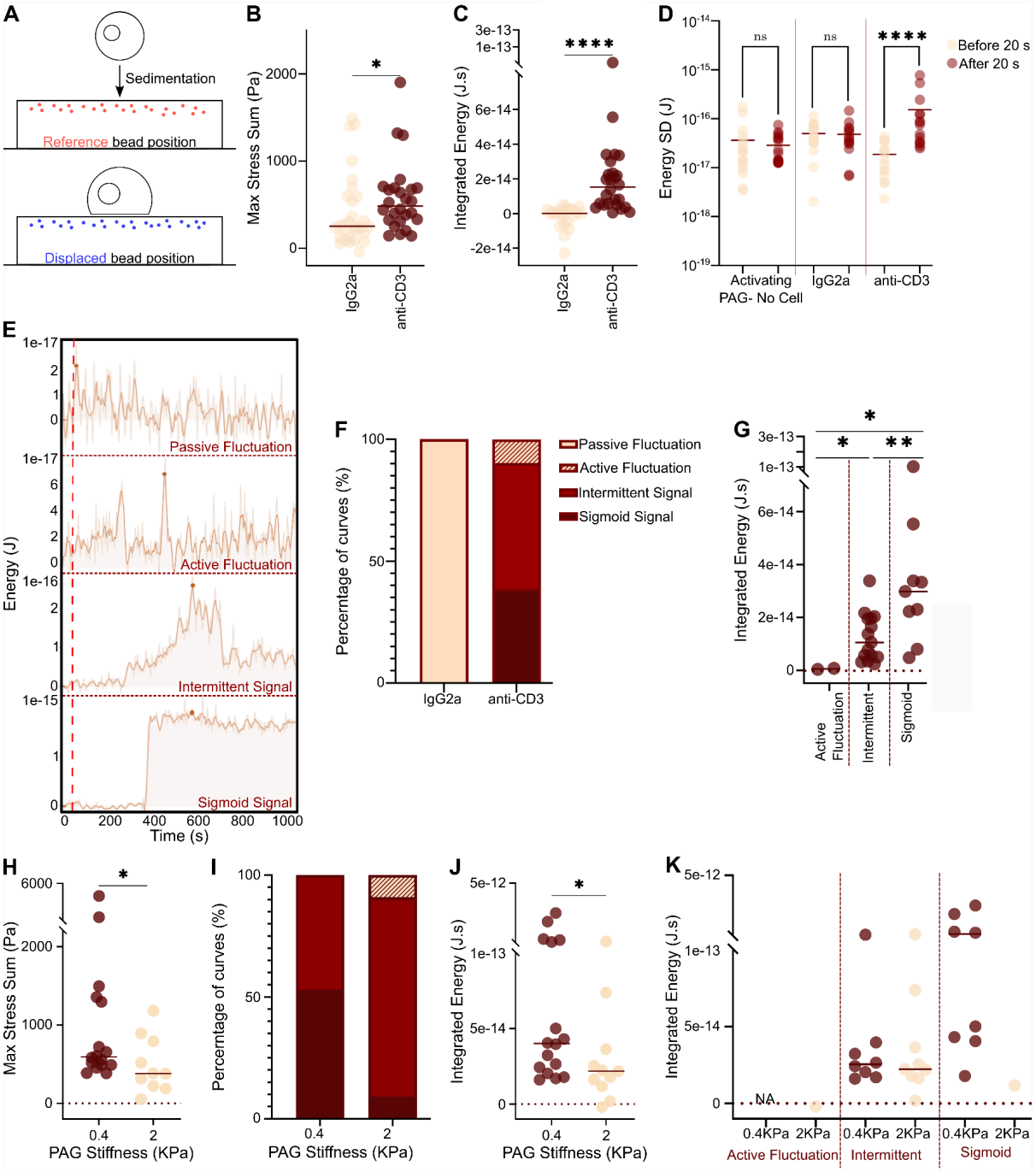
A
Sedimentation
Reference bead position
Displaced bead position
B
Max Stress Sum (Pa)
IgG2a
anti-CD3
C
Integrated Energy (J.s)
IgG2a
anti-CD3
D
Energy SD (J)
ns
ns
Before 20 s
After 20 s
Activating PAG- No Cell
IgG2a
anti-CD3
E
Energy (J)
Passive Fluctuation
Active Fluctuation
Intermittent Signal
Sigmoid Signal
Time (s)
F
Percentage of curves (%)
Passive Fluctuation
Active Fluctuation
Intermittent Signal
Sigmoid Signal
IgG2a
anti-CD3
G
Integrated Energy (J.s)
Active Fluctuation
Intermittent
Sigmoid
H
Max Stress Sum (Pa)
PAG Stiffness (KPa)
I
Percentage of curves (%)
PAG Stiffness (KPa)
J
Integrated Energy (J.s)
PAG Stiffness (KPa)
K
Integrated Energy (J.s)
NA
0.4KPa 2KPa 0.4KPa 2KPa 0.4KPa 2KPa
Active Fluctuation
Intermittent
Sigmoid

Figure 3

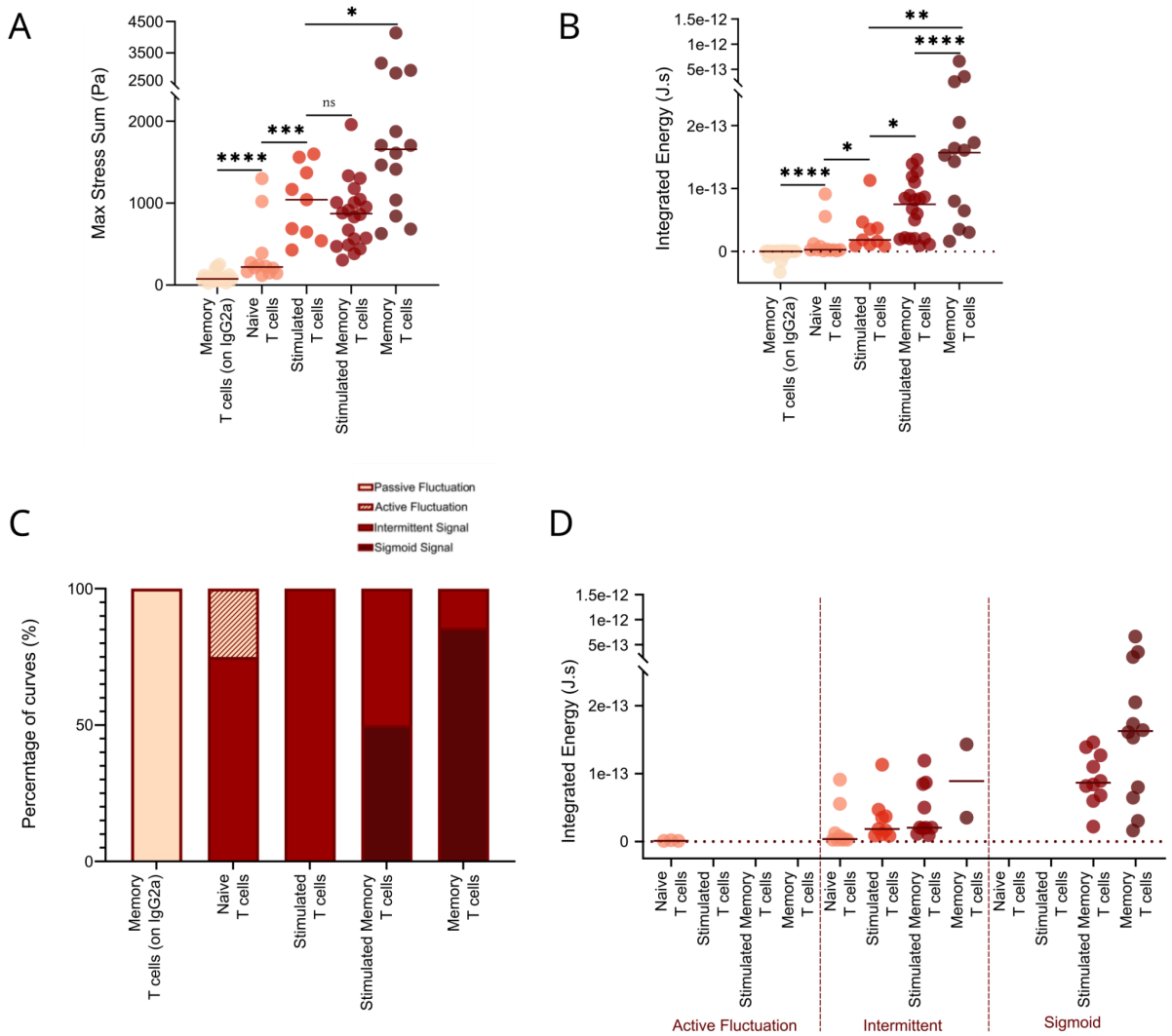
A
Max Stress Sum (Pa)
4500
3500
2500
2000
1000
0
****
***
ns
*
Memory T cells (on IgG2a)
Naive T cells
Stimulated T cells
Stimulated Memory T cells
Memory T cells
B
Integrated Energy (J.s)
1.5e-12
1e-12
5e-13
2e-13
1e-13
0
****
*
*
**
****
Memory T cells (on IgG2a)
Naive T cells
Stimulated T cells
Stimulated Memory T cells
Memory T cells
C
Passive Fluctuation
Active Fluctuation
Intermittent Signal
Sigmoid Signal
Percentage of curves (%)
100
50
0
Memory T cells (on IgG2a)
Naive T cells
Stimulated T cells
Stimulated Memory T cells
Memory T cells
D
Integrated Energy (J.s)
1.5e-12
1e-12
5e-13
2e-13
1e-13
0
Naive T cells
Stimulated T cells
Stimulated Memory T cells
Memory T cells
Active Fluctuation
Intermittent
Sigmoid